Reconstructing Open Surfaces via Graph-Cuts

Min Wan, Yu Wang, Egil Bae, Xue-Cheng Tai, and Desheng Wang

Abstract—A novel graph-cuts-based method is proposed for reconstructing open surfaces from unordered point sets. Through a Boolean operation on the crust around the data set, the open surface problem is translated to a watertight surface problem within a restricted region. Integrating the variational model, Delaunay-based tetrahedral mesh and multiphase technique, the proposed method can reconstruct open surfaces robustly and effectively. Furthermore, a surface reconstruction method with domain decomposition is presented, which is based on the new open surface reconstruction method. This method can handle more general surfaces, such as nonorientable surfaces. The algorithm is designed in a parallel-friendly way and necessary measures are taken to eliminate cracks and conflicts between the subdomains. Numerical examples are included to demonstrate the robustness and effectiveness of the proposed method on watertight, open orientable, open nonorientable surfaces and combinations of such.

Index Terms—Graph cuts, open surface, domain decomposition, Delaunay triangulation

1 Introduction

Reconstructing a surface from an unordered point data set has been a significant yet challenging problem in computer graphics for the last decade. As a critical step of creating computer graphics, surface reconstruction fills the gap between machine perception and machine understanding, i.e., the process from discrete scanned data to a continuous model. Due to the development of 3D scanners and the increasing demand of computer graphics, extensive research has been conducted in the surface reconstruction field, much of which was dedicated to the watertight surface reconstruction for its topological simplicity and desirable properties. Open surface reconstruction problems, however, occur often in real applications, such as incomplete scanned data. As a topic which has been overlooked, the open surface reconstruction problem, to some extent, has more significance than the watertight surface problem for its topological generality. The definitions of watertight and open surface are as follows:

A surface is defined as 2-manifold embedded in R^3. In our study, we restrict a surface to be a compact 2-manifold, which we are referring to by saying a watertight surface. An open surface is defined as a 2-manifold with boundary embedded in R^3. The boundary of a manifold S is denoted by ∂S. [1]

- *M. Wan and D. Wang are with the Division of Mathematical Sciences, School of Physical and Mathematical Sciences, Nanyang Technological University, 21 Nanyang Link, Singapore 637371. E-mail: wanm0003@e.ntu.edu.sg, desheng@ntu.edu.sg.*
- *Y. Wang is with CGGVeritas Co., CGGVeritas Building, 9 Serangoon, North Avenue 5, Singapore 554531. E-mail: Yu.Wang@cggveritas.com.*
- *E. Bae is with the Department of Mathematics, University of Bergen, Johaness Brunsgate 12, 5007 Bergen, Norway. E-mail: egil.bae@math.uib.no.*
- *X.-C. Tai is with the Division of Mathematical Sciences, School of Physical and Mathematical Sciences, Nanyang Technological University and the Department of Mathematics, University of Bergen, Johaness Brunsgate 12, 5007 Bergen, Norway. E-mail: tai@mi.uib.no.*

Manuscript received 11 July 2011; revised 16 Jan. 2012; accepted 22 Apr. 2012; published online 4 May 2012.
Recommended for acceptance by W. Wang.
For information on obtaining reprints of this article, please send e-mail to: tvcg@computer.org, and reference IEEECS Log Number TVCG-2011-07-0148.
Digital Object Identifier no. 10.1109/TVCG.2012.119.

Most surface reconstruction methods can be categorized into two groups, explicit methods and implicit methods. Explicit methods are mainly local geometric approaches based on Delaunay triangulation and dual Voronoi diagram such as Alpha shape and CRUST algorithm [2], [3], [4], [5], [6]. One advantage of these methods is their theoretical guarantee that there exists a subcomplex of Delaunay triangulation of the data set, which is homeomorphic to the ground-truth surface given a sufficient sampling. Since these methods are local approaches, the global topological characteristics such as watertight or open, will not affect their performances. Their target is the potential homeomorphic subcomplex embedded in the Delaunay triangulation. The topology of the subcomplex surface does not make any difference. Hence, the explicit method can handle quite a number of open surface cases.

However, the explicit methods are subject to many reconstruction difficulties such as nonuniformity, undersampling, and noises [3], [7], [8]. Hence, during the last decade, variational models were brought into the reconstruction field. The reconstruction problem is formulated as a minimization problem of an energy functional defined over surfaces. To minimize an energy functional with respect to the surface, a consistent parametrization of the surface is not always available during the optimization procedure. As a result, researchers turned to the implicit methods [8], [9], [10], [11], [12], [13], [14], [15], [16], [17], [18], [19], such as the level set method, to gain flexibility of representation and mathematical facilities. One important such level set approach based on solving the underlying partial differential equations was proposed by Zhao in [7], [11]. As an alternative, graph cuts can also minimize the energy functionals over implicitly defined surfaces, and has been successfully applied to the surface reconstruction problem in [20], [21], [22]. The main advantages of graph cuts are the efficiency and ability to find global minima. However, the competence of both the level set method and graph cuts is lost on more general topologies [23]. Some reconstruction methods have been proposed to handle open surfaces recently [18], [19], [22], [24], [25], [26] which work successfully in practice. However, the robustness or the efficiency is

still in study. To sum up, all these methods for open surfaces have some disadvantages and "*it is not clear how to devise methods for curves and surfaces that have ends or edges (respectively) within the computational domain*" [23].

In this paper, a novel variational reconstruction method for open surfaces is proposed. Unlike previous methods, our method separates the two types of ill posedness in the open surface problem and handles them sequentially in different ways. The explicit methods are adapted to handle the uncertainty of the surface boundary. The medial axis frequently used in the explicit methods are applied in a different manner. And the implicit method is used to tackle the uncertainty of the data connectivity issue, which contains various reconstruction difficulties such as undersampling and noises. This new methodology not only grants the merits from both explicit and implicit methods, but also provides approaches to more general cases such as the combination of open and watertight surfaces. Following is a description of our algorithm.

In the proposed method, the data set points as well as the properly generated background points are inserted to an unstructured tetrahedral mesh framework in a Delaunay way. In the tetrahedral mesh, a crust is established as the vicinity domain around the data set. A graph dual to the whole mesh is then built according to the energy functional and the minimization is achieved by applying max-flow/min-cut algorithms. To avoid trivial null result, it is necessary to specify boundary conditions before minimization. This can only be accomplished under the assumption that the domain can be separated into two or more subdomains by the watertight crust, which does not hold any more for an open surface problem.

To tackle this issue, a Boolean operation is proposed to restrict the region of interest within a narrow band. In the proposed method, two crusts with different thickness are built around the data set. The medial axis of the thick crust is to be obtained. One more crust is then built around the boundary of the medial axis. Subsequently, the two crusts around the data set are trimmed by the crust around the boundary. The trimmed thick crust can be separated by the trimmed thin crust. Hence, in the restricted region, i.e., the trimmed thick crust, the trimmed thin crust is watertight such that region growing algorithms and graph-cut techniques can be applied. More details and illustrations of this series of operations are provided in Section 3.

Furthermore, a surface reconstruction method based on domain decomposition is presented. The domain decomposition idea has been applied to computer vision [27], [28], [29]. Recently it is found also useful as a robust alternating minimization scheme between overlapped subspaces [30], [31]. In recent study, the dual graph could be subdivided into subgraphs as well to gain extra efficiency [32]. In the decomposition method, the whole domain is decomposed into several subdomains. The input data are then decomposed into subproblems to be approached separately. Certain measure is taken to eliminate cracks and conflicts effectively. The parallel efficiency may be undermined due to the interaction between subdomains. However, it can be compensated largely by a proper decomposition scheme. The method proposed can handle more general surfaces such as nonorientable surfaces. To the best of our knowledge, this is the first attempt to approach the nonorientable surface reconstruction problem via graph cuts.

The remainder of this paper is organized as follows: In Section 2, a brief review of watertight surface reconstruction based on Delaunay triangulation and graph cuts is given. Section 3 deals with the open surface problem. The new method to tackle this problem is proposed and the algorithm is given in details. Section 4 gives an important application, the surface reconstruction based on domain decomposition, which can handle more general surfaces. In Section 5, various numerical examples are presented to demonstrate effectiveness and robustness of the proposed method on all kinds of surfaces. Finally, Section 6 concludes the paper.

2 Graph-Cuts Reconstruction of Watertight Surface

In this section, a variational reconstruction method is reviewed for watertight surfaces based on graph cuts [33]. The cost energy functional is a generalization from the weighted minimal surface model [11], which is also related to the minimal surface [34] or geodesic active contours [35] approaches. This functional is minimized on an unstructured tetrahedral mesh framework, which provides more flexibility and effectiveness than structured grids used in other graph-based methods [21], [22], [36]. As a matter of fact, the Delaunay-based mesh guarantees the existence of a subcomplex homeomorphic to the ground-truth surface given a sufficient sampling. The method can handle various reconstruction difficulties such as noise, undersampling, and nonuniformity. By adopting the idea presented in [37], the method is able to address two phase and multiphase problems in a unified approach. A brief review of the ideas and techniques on watertight surfaces will be given in this section.

2.1 Two Phase Surface Reconstruction via Graph Cuts

For convenience, this section only discusses two phase problems, in which the ground-truth surface S simply separates the embedding domain $X \subset R^3$ into two regions. Let P be a point data set approximately sampled from S in the domain X. Define the distance function as $d(x) = d(x, P) = \inf_{y \in P} d(x, y)$, where $d(x, y)$ is the euclidean distance between points x and y in R^3. As in [11], [33], the following cost energy is proposed for surface reconstruction:

$$E(\Gamma) = \int_X |\phi_\Gamma(x) - I(x) \mid \beta(x)dx + \int_\Gamma d(x)ds + \alpha \int_\Gamma ds,$$

where Γ is an arbitrary surface and $\int_\Gamma ds$ is the surface integral over Γ. $\phi_\Gamma(x)$ is the piecewise constant level set function with regard to Γ; $I(x)$ is the indicator function prespecifying the level set values; $\beta(x)$ is the confidence function suggesting the faithfulness of $I(x)$; α is the regularization coefficient. The definitions of these functions are given as follows:

- $\phi_\Gamma(x)$ is the piecewise constant level set function same as [38] corresponding to the surface Γ

$$\phi_\Gamma(x) = \begin{cases} c_1 & \text{if } x \in \text{interior of } \Gamma \\ c_2 & \text{if } x \in \text{exterior of } \Gamma, \end{cases} \quad (1)$$

where c_1 and c_2 serve as the constant level set value and could be any distinct constants. As a consequence, the surface Γ is implicitly represented as the discontinuities of $\phi_\Gamma(x)$.

- The crust around the input data P is defined as $C_d^P = \{x \in X : d(x,P) \le d\}$. C_d^P partitions the whole domain into two regions given a ϵ-sample P sampled from a watertight surface [3]

$$I(x) = \begin{cases} 0 & \text{if } x \in C_d^P \\ c_1 & \text{if } x \text{ is bounded by } C_d^P \\ c_2 & \text{if } x \text{ is unbounded by } C_d^P, \end{cases} \tag{2}$$

  where $I(x)$ is the indicator function prespecifying the level sets. Compared with final level set $\phi_\Gamma(x)$, $I(x)$ serves as a boundary condition. If x is contained in the set bounded by C_d^P (interior part of $X \backslash C_d^P$), x is said to be bounded by C_d^P; if x is contained in the set unbounded by C_d^P (exterior part of $X \backslash C_d^P$), x is said to be unbounded by C_d^P.
- $\beta(x)$ is the confidence function suggesting the faithfulness of $I(x)$ as an estimate for $\phi_\Gamma(x)$

$$\beta(x) = \begin{cases} 0 & \text{if } x \in C_d^P \\ \sigma & \text{others,} \end{cases} \tag{3}$$

  where σ is a relatively large positive value. With this confidence function weighted on $|\phi_\Gamma(x) - I(x)|$, the reconstructed surface would fall in the crust region.

The first term in (1), can be thought of as specifying boundary conditions of ϕ_Γ. It constrains the result surface within the crust region, i.e., C_d^P. Otherwise, if there were any disagreements between $\phi_\Gamma(x)$ and $I(x)$ out of C_d^P, the energy would not be minimized. This term is important; without it the global minimum of (1) would be the trivial null surface, i.e., ϕ_Γ is just a constant everywhere.

The second term is the essential part in the weighted minimal surface model [11] and the third term is the regularization term concerning the surface area. By tuning the regularization coefficient α, a compromise between faithfulness and smoothness can be achieved.

In this method, (1) is discretized on an unstructured tetrahedral mesh $\mathcal{T}_h$ instead of structured grids used in other graph-based methods. And a mesh and triangulation are referring to the same thing [39]. Generally, a mesh $\mathcal{T}_h$ can be defined by a pair (V, C). V is the set of all vertices and C is a complex consisting of four types of simplexes, i.e., vertices, edges, triangles, and tetrahedra. For vertices u, v, w, z, we define $\{v, u\}$ as the edge between v and u, $\{v, u, w\}$ as the triangle with vertices v, u, w, and $\{v, u, w, z\}$ as the tetrahedron with vertices v, u, w, z. $\{K_i\}_{i=1}^N$ are used to denote all N tetrahedra in $\mathcal{T}_h$. In our case, V is the set of mesh points including data points and background points $P \cup Q$.

In a mesh $\mathcal{T}_h$, we can define 1-ring neighborhood of a vertex v as $N_v^1 = \{u | \{v, u\} \in C\}$ and M-ring neighborhood in a recursive way

$$N_v^M = \left\{u | \exists w \in N_v^{M-1}, \{w, u\} \in C\right\}. \tag{4}$$

Based on this neighborhood system, the crust around the data set P can be defined as

$$K_M^P = \left\{K_i | \exists v \in K_i, v \in N_u^M, u \in P\right\}. \tag{5}$$

Given P, the sizing function $h(v)$ for each vertex $v \in P$ can be defined as the $d(v, P \backslash \{v\})$: the closeness measure to the other vertices. Under uniformity assumption, the average sizing function $\bar{h} = \sum_{v \in P} v(h)$ could well approximate that of each individual vertex. The background points aim to construct the mesh of reasonable size and good quality. Either regular grid or Body-centered cubic (BCC) lattice is a good choice

$$BCC(h) = h \cdot \left(\mathbb{Z}^3 \cup \left(\mathbb{Z}^3 + \left(\frac{1}{2}, \frac{1}{2}, \frac{1}{2}\right)\right)\right), \tag{6}$$

where $\mathbb{Z}^3$ are points with integer coordinates and h is the size of BCC lattice [40]. The background point set is defined as $Q = \{v | v \in BCC(\bar{h}) \cap X, d(v, P) > \bar{h}\}$. The restricting inequality $d(v, P) > \bar{h}$ is necessary since too close background points would destroy the ground truth embedded in the mesh.

When the data sets are nonuniform, i.e., with widely varying sizing function values, the uniform background lattice points are not suitable any more. A well-graded sizing mesh is required instead. The mesh element sizes shall conform with the local sizing function. The parameter h of $BCC(h)$ shall vary correspondingly. A good meshing technique is [41], which utilized octree to construct graded BCC meshes. More advanced nonuniform mesh generation technique is also available, see [42]. The benefit of such a reasonable sized mesh will be seen later.

In this mesh framework, the surface Γ can be approximated by Γ_h, a subcomplex of $\mathcal{T}_h$. Amenta et al. [3] show that there exists a subcomplex of the Delaunay triangulation of P, which is homeomorphic to the ground-truth surface S. As an extension, Wan et al. [43] show that this homeomorphic subcomplex still exists in the Delaunay triangulation of $P \cup Q$ if given a reasonable distribution of Q.

The first term in (1), the integral over the whole domain X can be simply discretized as

$$\begin{aligned} &\int_X |\phi_\Gamma(x) - I(x)| \beta(x) dx \\ &= \sum_{i=1}^N \int_{K_i} |\phi_\Gamma(x) - I(x)| \beta(x) dx \\ &\approx \sum_{i=1}^N |\phi_{\Gamma_h}(K_i) - I(K_i)| \beta(K_i), \end{aligned} \tag{7}$$

$$\phi_{\Gamma_h}(K_i) = \begin{cases} c_1 & \text{if } K_i \in \text{interior of } \Gamma_h \\ c_2 & \text{if } K_i \in \text{exterior of } \Gamma_h, \end{cases} \tag{8}$$

$$I(K_i) = \begin{cases} 0 & \text{if } K_i \in K_M^P \\ c_1 & \text{if } K_i \text{ is bounded by } K_M^P \\ c_2 & \text{if } K_i \text{ is unbounded by } K_M^P, \end{cases} \tag{9}$$

$$\beta(K_i) = \begin{cases} 0 & \text{if } K_i \in K_M^P \\ \sigma & \text{others,} \end{cases} \tag{10}$$

where σ is a relatively large positive value.

The second and third terms in (1) are surface integrals. The surface triangulation Γ_h can be thought of as the union of the triangular faces shared by tetrahedra with different level set values

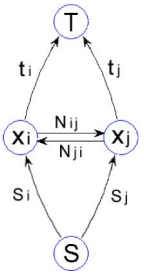

Fig. 1. Graph edge weight assignment.

$$\Gamma_h = \bigcup_{\phi_\Gamma(K_i)\neq\phi_\Gamma(K_j)} \Gamma_{ij},$$

where $\Gamma_{ij} = K_i \cap K_j$. Hence, combining (7), (1) can be discretized as follows:

$$\begin{aligned} E(\Gamma) \approx & \sum_{i=1}^{N} |\phi_{\Gamma_h}(K_i) - I(K_i)|\beta(K_i) \\ & + \sum_{i,j} (d_{ij} + \alpha) S_{ij} \mathbf{1}_{\{\phi_{\Gamma_h}(K_i)\neq\phi_{\Gamma_h}(K_j)\}}, \end{aligned} \tag{11}$$

where

$$d_{ij} = \frac{\int_{\Gamma_{ij}} d(x)ds}{\int_{\Gamma_{ij}} ds} \qquad S_{ij} = \int_{\Gamma_{ij}} ds. \tag{12}$$

The energy of $E(\Gamma)$ can be minimized efficiently by graph-cuts, since this energy functional is graph representable, which can be verified by the conclusion in [44]. First, a graph dual to the primal tetrahedral mesh is constructed, in which each node corresponds to a tetrahedron in the mesh and each edge corresponds to a triangular face in the mesh.

The edge weights are determined by different terms in $E(\Gamma)$ as shown in Fig. 1 and below

$$\begin{aligned} & s_i = |I(K_i) - c_2|\beta(K_i), \quad t_i = |I(K_i) - c_1|\beta(K_i) \\ & N_{ij} = (d_{ij} + \alpha)S_{ij}, \quad N_{ji} = (d_{ij} + \alpha)S_{ij}. \end{aligned} \tag{13}$$

After graph construction, max-flow/min-cut algorithms can be applied on the obtained graph. The algorithm in [45] is a good choice for its empirically good performance. Due to the primal-dual relationship in Table 1, the reconstructed surface can be directly extracted from the background mesh according to the minimal cut. The flow chart is shown in Fig. 2.

2.2 Multiphase Reconstruction via Graph Cuts

We assume now that the interior and exterior of the surface are not connected sets. Such cases can be handled by introducing more labels. We assume the surface separates X into M connected regions $\{X_i\}_{i=1}^{M}$. Surfaces of this kind can be represented in the level set framework of [38] by defining ϕ_Γ as $\phi_\Gamma(x) = c_i$ for $x \in X_i$, $i = 1, \ldots, M$. As before, Γ is

TABLE 1
Relationship between Cut and Surface

Cut in dual graph	Surface in primal mesh
$C = \bigcup_{x_i,x_j\in V,\ \phi_i\neq\phi_j} (x_i, x_j)$	$\Gamma = \bigcup_{K_i,K_j\in\mathcal{T}_h,\ \phi_i\neq\phi_j} (K_i \cap K_j)$

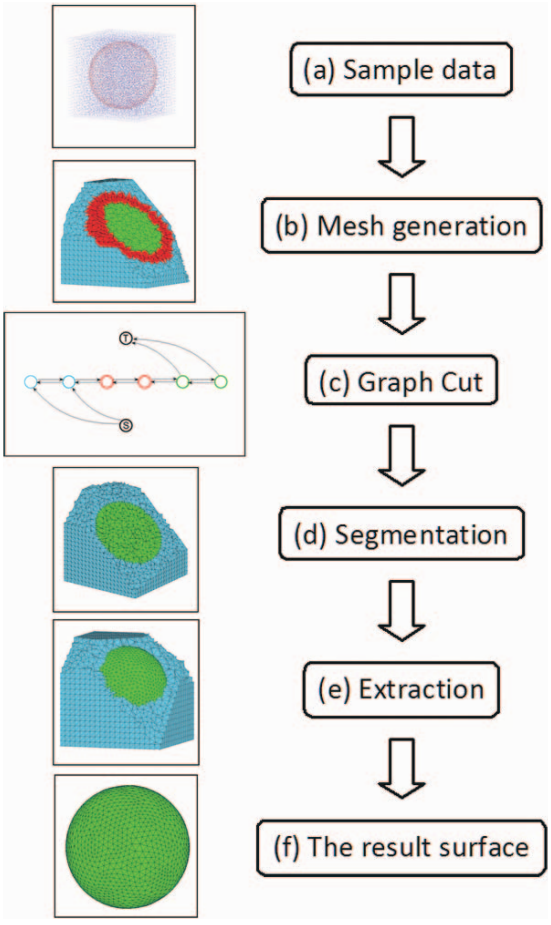

Fig. 2. Watertight surface reconstruction. Given a data set (a) sampled from an object surface, proper background points such as grid points are generated according to the data points distribution. An unstructured tetrahedral mesh (b) is generated in a Delaunay way and the crust around the data set is established. A graph dual to the mesh is constructed (c). Graph-cuts are applied and segmentation on the primal mesh is obtained (d). Extract the surface from tetrahedral mesh (e), the reconstructed surface is obtained (f).

represented as the discontinuities of ϕ_Γ. The complete energy functional (1) is therefore given in the discrete setting as

$$\begin{aligned} E(\Gamma) \approx & \sum_{i=1}^{N} |\phi_{\Gamma_h}(K_i) - I(K_i)|\beta(K_i) \\ & + \sum_{i,j} (d_{ij} + \alpha) S_{ij} \mathbf{1}_{\{\phi_{\Gamma_h}(K_i)\neq\phi_{\Gamma_h}(K_j)\}}, \end{aligned} \tag{14}$$

where

$$d_{ij} = \frac{\int_{\Gamma_{ij}} d(x)ds}{\int_{\Gamma_{ij}} ds}, \qquad S_{ij} = \int_{\Gamma_{ij}} ds. \tag{15}$$

Minimization problems involving multiple phases, or labels, have been studied previously in image processing. For instance, in image segmentation, each phase represents a region and the minimization problem has exactly the form of (14), but with a different data cost function. Such problems are known to be NP-hard and cannot in general be solved exactly. Instead one can solve the problem approximately, typically via the alpha expansion algorithm [46]. However, it is known alpha expansion does not work so well when the data costs are weak, which is the case for our problem (14),

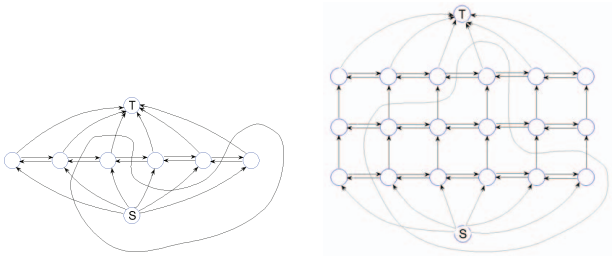

(a) two phase segmentation (b) multiphase segmentation

1	1	2	1	1	2

(c) two phase segmentation result

1	3	3	4	2	2

(d) multiphase segmentation result

Fig. 3. One dimensional example to illustrate multilayer graph [37].

where the data terms are all zero within the crust. We will instead follow the work of Ishikawa [47] and a later modification [37], by efficiently solving a simpler approximate problem via graph cuts. By making a simplification of the length term in (14), we can convert the problem (14) into a graph representable form. The simplification does not seem to introduce any noticeable errors in our experiments. It was observed that several surfaces could be represented by a hypersurface in a higher dimensional domain. An extra "dimension" is introduced along with the original graph dual to the primal mesh. This multilayer graph idea is illustrated in Fig. 3.

The multilayer idea does not change much from image processing to surface reconstruction. As earlier, we let C_d^P denote the crust around the data points P. The domain $X \backslash C_d^P$ now contains several disconnected subdomains (instead of just two as in the last section). The indicator function I should be specified such that it takes different values in different subdomains

$$I(x) = \begin{cases} 0 & \text{if } x \text{ in } C_d^P \\ c_i & \text{if } x \text{ inside the } i\text{th subdomain.} \end{cases} \tag{16}$$

Once the original graph dual to the primal mesh is constructed, it is duplicated $M-1$ times if the number of subdomains is M. More specifically, a graph is created such that $M-1$ vertices in the vertex set are associated to each tetrahedra K_i. The notation v_i^k is used for the vertex corresponding to K_i at level $k \in \{1, \ldots, M-1\}$. We let $c(a,b)$ denote the cost on the edge between vertex a and b. The edges connecting vertices in the same level are called horizontal edges, while the others are called vertical edges. The weights for the vertical edges represent the data term, and are defined by

$$\begin{aligned} c\big(s, v_i^1\big) &= |c_1 - I(K_i)|\beta(K_i) \ \text{ for } \ i = 1, \ldots, N, \\ c\big(v_i^k, v_i^{k+1}\big) &= |c_{k+1} - I(K_i)|\beta(K_i) \ \text{ for } \ i = 1, \ldots, N, \\ &\qquad \forall k \in \{1, \ldots, M-2\}, \\ c\big(v_i^{M-1}, t\big) &= |c_M - I(K_i)|\beta(K_i) \ \text{ for } \ i = 1, \ldots, N. \end{aligned} \tag{17}$$

The weights for the horizontal edges represent the regularization term in functional (1), and are defined as follows:

$$c\big(v_i^k, v_j^k\big) = (d_{ij} + \alpha)S_{ij}, c\big(v_j^k, v_i^k\big) = (d_{ij} + \alpha)S_{ij}, \tag{18}$$

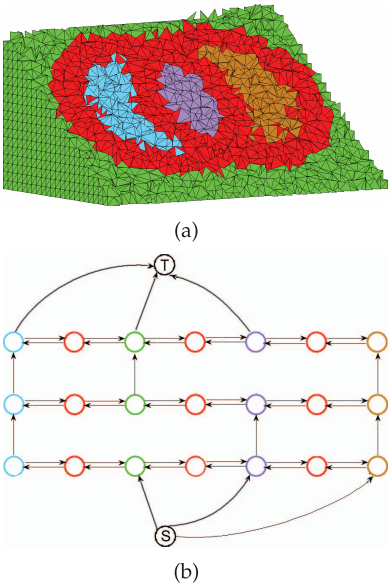

(a)

(b)

Fig. 4. A multiphase surface problem and the corresponding multilayer graph [33].

$$\forall i, j \in \{1, \ldots, N\}, \ \ \forall k \in \{1, \ldots, M-1\}.$$

After finding the minimum cut $\mathcal{C}$ on this graph, the labeling function can be recovered by

$$\phi_i = \begin{cases} c_1 & \text{if } \ \big(s, v_i^1\big) \in \mathcal{C} \\ c_{k+1} & \text{if } \ \big(v_i^k, v_i^{k+1}\big) \in \mathcal{C}, \ \ k = 1, \ldots, M-2 \\ c_M & \text{if } \ \big(v_i^{M-1}, t\big) \in \mathcal{C}. \end{cases} \tag{19}$$

As shown in Fig. 4, the multilayer graph idea is illustrated by two intersecting spheres. Fig. 4a presents the cut view of the mesh. The three layer graph is shown in Fig. 4b. The nodes in the graph correspond to the tetrahedra with the same color. The weights distribution among vertical edges depend on $I(K_i)$.

3 Open Surface Reconstruction via Graph Cuts

The method discussed in Section 2 can reconstruct watertight surfaces, which has an interior and exterior region in R^3. In this section, we discuss open surfaces, which obviously does not have a clear interior and exterior. One critical step of the previous method was the specification of the indicator function $I(x)$ as the establishment of the boundary conditions, which was completed by a phase detector based on region growing algorithms [48]. If the crust around the data set fails to separate the domain into two or more partitions as in Fig. 2b, the phase detector would label all regions out of the crust with the same indicator value. A solid and reasonable boundary condition is not available and hence the global minimum would be the trivial null surface. Fig. 5 illustrates this situation and the failure of our previous method by an example in two dimensions.

Certain interactive methods can be applied such as manually specifying the boundary condition. These methods apparently lack generality for more general cases. In this paper, a more intelligent and robust reconstruction method is proposed for general surfaces, including open

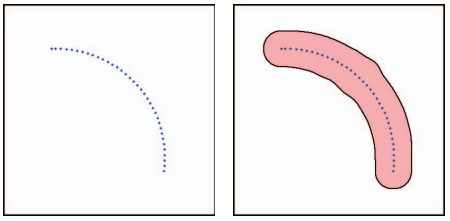

Fig. 5. The failure of previous graph-based methods.

surfaces, watertight surfaces, and combinations of such. The proposed method consists of an automatic partitioning procedure followed by all steps contained in Section 2. By defining a Boolean operation on the vicinity of the data set, the region of interest has been trimmed in such a way that it can be separated into two or more partitions by a watertight crust. Subsequent phase detection and graph techniques can be applied on the trimmed region. Detailed description is as follows.

3.1 A Description of the Method

The proposed method is briefly described as following steps:

1. Two crusts with different thickness parameters $d_1 < d_2$ are constructed around P: $C^P_{d_1}$ and $C^P_{d_2}$. These two crusts are illustrated in Fig. 6a, the dark red crust for $C^P_{d_2}$ and the light red one $C^P_{d_1}$.
2. The medial axis M_d of $\partial C^P_{d_2}$ is found. ∂M_d is denoted by Bd.
3. The crust around Bd is constructed: $C^{Bd}_{d_3}$, $d_3 \geq d_2$. Two crusts around P are trimmed by the crust around Bd. $\widetilde{C}^P_{d_1} = C^P_{d_1} - C^{Bd}_{d_3}$, $\widetilde{C}^P_{d_2} = C^P_{d_2} - C^{Bd}_{d_3}$. The gray balls stand for $C^{Bd}_{d_3}$ in Fig. 6b.
4. The phase detection based on region growing can be performed in $\widetilde{C}^P_{d_2}$ and graph cuts is applied to obtain the result surface. These two steps are shown in Figs. 6c and 6d.

In the proposed method, $\widetilde{C}^P_{d_2}$ rather than the whole domain X is the region of interest. $\widetilde{C}^P_{d_2}$ can be separated into two or more partitions by $\widetilde{C}^P_{d_1}$, which equivalently translates the open surface problem to a watertight one.

The medial axis of a manifold $\Sigma \subset R^k$ is the closure of the set of points in R^k that have at least two closest points in Σ [3]. The medial axis M_d itself is a good approximation to the ground-truth surface S. Hence, ∂M_d well approximates ∂S. In three dimensions, the medial axis of a two manifold could be the collection of surfaces, curves or even vertices. The topology of the medial axis of a general manifold is still an open problem. However, the manifold we are discussing is $\partial C^P_{d_2}$, a dilated version of S. Finding the medial axis of $\partial C^P_{d_2}$, a procedure also known as skeletonization, is an inverse transformation of the dilation. This fact as well as S being a two manifold largely eliminates the transdimensional issues of the medial axis.

d_1, d_2, and d_3 serve as the thicknesses for three crusts used in the proposed method. The discussion of these parameters setting and their impact is given as follows: 1) d_1 is the thickness of the inner crust $C^P_{d_1}$. Under noise-free assumption, $d_1 > \min_{v \in P} h(v)$, where $h(v)$ is the sizing function defined in Section 2. This restriction means the $C^P_{d_1}$ shall

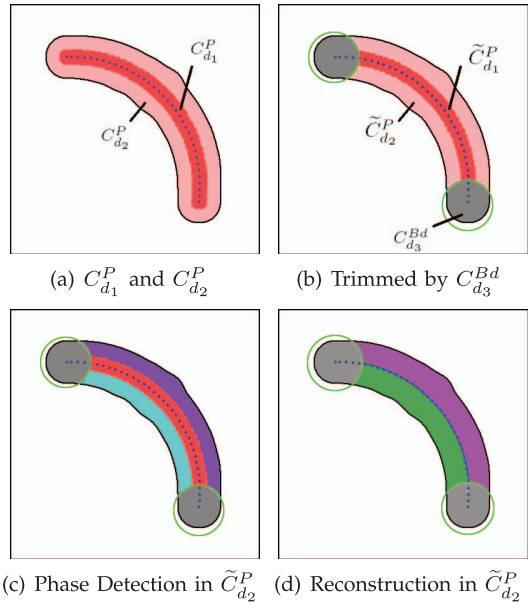

(a) $C^P_{d_1}$ and $C^P_{d_2}$ (b) Trimmed by $C^{Bd}_{d_3}$

(c) Phase Detection in $\widetilde{C}^P_{d_2}$ (d) Reconstruction in $\widetilde{C}^P_{d_2}$

Fig. 6. Crust establishments and Boolean operation.

connect any data point to at least another data point. On uniform and noise-free cases, we usually set $d_1 = 2\bar{h}$. 2) d_2, as the thickness of the outer crust $C^P_{d_2}$, is only required be slightly larger than d_1 in continuous circumstance, usually set to $4\bar{h}$. 3) d_3 is the thickness of the trimming crust $C^{Bd}_{d_3}$, which is required to be slightly larger than d_2, both in continuous and discrete circumstances. It is set to $5\bar{h}$ in the experiments. When facing a nonuniform data set, a single tuple of d_i parameters obviously is not enough. $\{d_i, i = 1, 2, 3\}$ shall vary according to the data density, which means the $\bar{h}$ shall be replaced by the local $h(v)$.

It is worth noticing that Bd would be an empty set if the ground-truth surface S is watertight. Therefore, an empty crust $C^{Bd}_{d_3}$ is constructed and no Boolean operation is done upon $C^P_{d_1}$ and $C^P_{d_2}$. In other words, the method in Section 2 is a special case of the proposed method. Various types of cases, including open, watertight, and hybrid surfaces, can be approached by a single algorithm without any a priori knowledge of surface topology or beforehand hole detections.

3.2 The Implementation of the Method

In this section, we provide the discrete versions of the concepts involved in the above algorithm. This algorithm is implemented upon a tetrahedral mesh based on these discrete concepts.

A tetrahedral mesh $\mathcal{T}_h$ is generated as the Delaunay triangulation of $P \cup Q$, P the input data, and Q the background points. In $\mathcal{T}_h$, the discrete distance is defined $d_h(v, u) = \min_M \{M | v \in N^M_u\}$, via neighborhood definition in (4).

Given a triangulated two manifold Σ_h, the medial axis vertices are defined as the collection of the vertices, whose distance to Σ_h is realized by at least two points in Σ_h: $M_V = \{v | \exists u_1, u_2 \in \Sigma, d_h(v, u_1) = d_h(v, u_2) = d_h(v, \Sigma)\}$. The discrete medial axis is the subcomplex of $\mathcal{T}_h$, whose underlying vertices are M_V. $M_F = \{\triangle uvw | u, v, w \in M_V\}$.

TABLE 2
Open Surface Reconstruction on a Tetrahedral Mesh

Inputs	A point set P
Algorithm	
1.	Mesh generation: $\mathbf{Del}(P \cup Q)$
2.	Build crusts: $K^P_{N_1}$, $K^P_{N_2}$
3.	Find M_F, the medial axis of $\partial K^P_{N_2}$.
4.	Find $Bd = \partial M_F$
5.	Build crust: $K^{Bd}_{N_3}$
6.	Trim crusts: $\widetilde{K}^P_{N_1} = K^P_{N_1} - K^{B_d}_{N_3}$, $\widetilde{K}^P_{N_2} = K^P_{N_2} - K^{B_d}_{N_3}$
7.	Region growing in $\widetilde{K}^P_{N_2}$
8.	Apply graph-cuts
Outputs	The surface triangulation S

Recall the discrete crust definition in (5). $C^P_{d_1}$, $C^P_{d_2}$, and $C^{Bd}_{d_3}$ are translated to $K^P_{N_1}$, $K^P_{N_2}$, and $K^{Bd}_{N_3}$. The integers N_1, N_2, and N_3 play the roles of thickness parameters instead. In this way, the effect of nonuniformity could be absorbed by the adaptive mesh. Meanwhile the varying $\{d_i\}$ parameters could be replaced by the fixed $\{N_i\}$ parameters.

Based on these definitions in a discrete language, the proposed algorithm can be effectively implemented on a tetrahedral mesh as described in Table 2. The underlying Delaunay-based mesh makes the resulting surface more likely to be homeomorphic to the ground truth. More examples are shown in Section 5 to demonstrate the effectiveness and robustness of the proposed method.

4 Reconstruction of Open Surfaces Based on Domain Decomposition

In Section 3, the open surface reconstruction method has been proposed, whose effectiveness and robustness will be shown in Section 5. The good performance on various kinds of surfaces leads to further consideration of its applications. One of the most significant applications is to reconstruct a surface based on domain decomposition. Domain decomposition has been successfully applied on computer vision field for a long time. One option is to use domain decomposition idea as preconditioners to get fast solvers for some related linear problems [27], [28], [29]. Some recent analysis reveals that domain decomposition can be used as a robust alternating minimization scheme between overlapped subspaces, see [30], [31]. In surface reconstruction, the robustness and effectiveness of such kind of divide-and-conquer algorithms will strongly depend on a good reconstruction method for general surfaces, since the surface in a subdomain may be open or have disconnected interior. Hence, based on the method proposed in Section 3, we present a reconstruction method based on domain decomposition. Since the idea of parallel surface reconstruction is also very attractive, the method is designed in such a way that it can easily be adapted to parallel machines.

Another motivation is the incompetence of the method proposed in Section 3 on some special cases. As is known, all 2-manifolds without boundary in R^3, i.e., watertight surfaces, are orientable [1]. The methods dedicated to watertight surfaces do not have to face the difficulty about nonorientability. However, the 2-manifolds with boundaries, i.e., open surfaces, may be nonorientable. This nonorientable surface problem would be a great challenge for those methods based on implicit representations. For instance, the method proposed in Section 3 cannot handle nonorientable surfaces such as Mobius strip. After the trimming operation, $\widetilde{C}^P_{d_1}$ may still fail to separate $\widetilde{C}^P_{d_2}$ into two or more subdomains. A surface reconstruction method based on domain decomposition would be helpful when facing this difficulty. Once the domain X has been decomposed properly, the surface piece in each subdomain is orientable, and can be approached by the method in Section 3. To the best of our knowledge, this study is the first to reconstruct nonorientable surfaces via graph cuts.

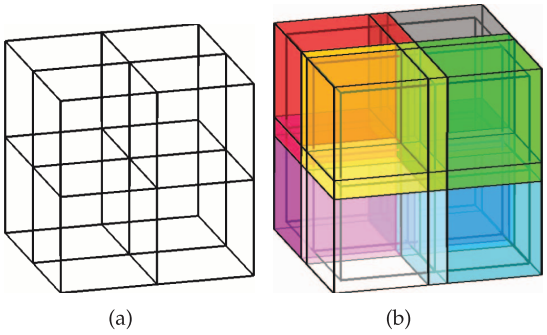

Fig. 7. Nonoverlapping and overlapping decomposition schemes.

4.1 Overlapping Domain Decomposition Scheme

Given a domain $X \subset R^3$, a partitioning $\{X_i\}_{i=1}^N$ of X can be obtained according to a decomposition scheme. In practice, the decomposition scheme can be spatially oriented or data oriented. In this study, a common spatial decomposition scheme is used. Obviously, any rectangular cuboid B can be decomposed into small tessellating rectangular cuboids $\{B'_i\}_{i=1}^N$ as illustrated in Fig. 7a. In our problem, by choosing B to be a rectangular cuboid properly bounding X, i.e., $X \subset B$, $\{X'_i\}_{i=1}^N$ can be obtained through $X'_i = X \cap B'_i$. Notice that $\cup_{i=1}^N X'_i = X$, $X'_i \cap X'_j = \emptyset$.

However, to avoid the cracks between subdomains, overlapping parts are necessary. In our study, an overlapping decomposition scheme could be obtained by expanding cuboid cells $\{B'_i\}_{i=1}^N$ to $\{B_i\}_{i=1}^N$ as shown in Fig. 7b. A new partitioning with overlapping $\{X_i\}$ is then obtained. The surface reconstruction problem on P is decomposed into the subproblems of $P_i = P \cap X_i$. To tackle the issue of possible conflicts and cracks in overlapping part, in this study, a sequential fix-the-boundary method is proposed. As a result, some parallel potential is lost due to the interaction between neighboring subdomains, which is discussed in the later section.

4.2 Fix-the-Boundary Reconstruction Method

Without loss of generality, assume that there are only two overlapping subdomains, i.e., X_i and X_j. The overlapping region is $X_{ij} = X_i \cap X_j$. We present our algorithm as following steps and illustrate them in Fig. 8.

1. In X_i, apply the method in Section 3 to the subproblem, i.e., reconstructing a surface S_i from $P_i = P \cap X_i$, as shown in Fig. 8a. Meanwhile, the background points falling in the overlapping region,

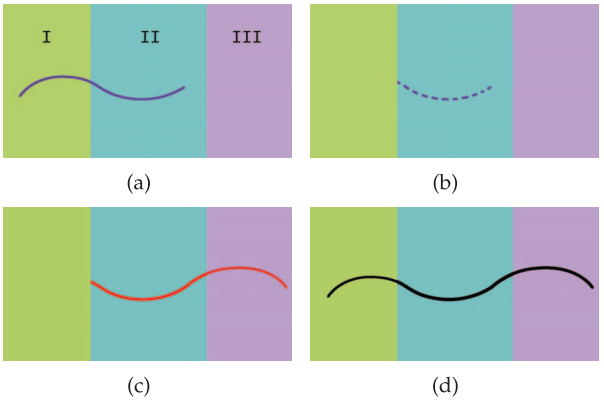

Fig. 8. A sequential fix-the-boundary method is presented to tackle cracks and conflicts. $X_i : I + II$; $X_j : II + III$; $X_{ij} : II$.

i.e., $Q_i \cap X_{ij}$, are stored. As well, the reconstructed surface in this region, i.e., $S_i \cap X_{ij}$, is recorded as shown in Fig. 8b.

2. In X_j, the subproblem of $P_j = P \cap X_j$ is solved with two modifications. The result surface is S_j as in Fig. 8c.
   a. Q_j, the original background points in X_j, is modified: $Q_j^{'} = (Q_j - X_{ij}) \cup (Q_i \cap X_{ij})$. The mesh is generated based on the modified $Q_j^{'}$.
   b. The graph in solving the subproblem is modified: the weights of edges dual to the faces in $S_i \cap X_{ij}$ are reduced to zero.
3. At last, merge these two surface patches and obtain the final output for the whole problem: $S = S_i \cup S_j$ as in Fig. 8d.

The modification on Q_j ensures that background points in overlapping region are identical for two subproblems, i.e., $Q_i \cap X_{ij} = Q_j^{'} \cap X_{ij}$. Under the assumption of general positions, the Delaunay triangulation of a point set is unique. Combined with the local property of Delaunay triangulations, it is safe to assert that the meshes in the overlapping region for two subdomains are identical, i.e., $\mathcal{T}_i \cap X_{ij} = \mathcal{T}_j \cap X_{ij}$.

The edge weight adjustment on graph in X_j makes the min-cut contains those adjusted edges, which correspond to the faces in $S_i \cap X_{ij}$. Equivalently, the reconstructed surface would contain $S_i \cap X_{ij}$. This efficiently eliminates conflicts and cracks. We refer to the edge weight adjustment as "fix the surface in X_{ij}" for short. The whole algorithm is given in Table 3.

4.3 Parallel Feasibility and Efficiency

As mentioned, some parallel potential is lost due to the interaction between subdomains in this method. Two neighboring subdomains cannot be processed simultaneously. To adapt this method to parallel machines, all subdomains shall be colored such that no neighboring subdomains have the same color. An identical color shared by subdomains suggests their independence and the feasibility to be processed simultaneously. The sequential algorithm in Table 3 could be adapted to a parallel one.

In 2D problems such as image segmentation [49], the well-known four-color theorem can limit the number of the colors required within four. Unfortunately, there is no such

TABLE 3
Reconstruction Based on Domain Decomposition

Inputs		
	1.	A point set P
	2.	Partition of X, $\{X_i\}_{i=1}^N$
Algorithm		
	1	For $i = 1 : N$
	2	$P_i = P \cap X_i$
	3	Generate Q_i according to P_i
	4	For each j, s.t. $X_i \cap X_j \neq \emptyset$
	5	If $F_{ij} == 1$
	6	$Q_i = (Q_i - X_{ij}) \cup Q_{ij}$
	7	Else
	8	$Q_{ij} = Q_{ji} = Q_i \cap X_{ij}$
	9	End If
	10	End For
	11	Mesh generation: $\mathbf{Del}(P_i \cup Q_i)$
	12	For each j, s.t. $X_i \cap X_j \neq \emptyset$
	13	If $F_{ij} == 1$
	14	Fix all S_{ij} in X_{ij}
	15	Else
	16	$F_{ij} = F_{ji} = 1$
	17	End If
	18	End For
	19	Graph-cuts and obtain S_i
	20	End For
Outputs		The surface triangulation $S = \bigcup_{i=1}^{N} S_i$

theoretic bound in three dimensions. For some special decomposition schemes, however, we can still find such color number bounds. For instance, regrading the 26-neighborhood regular grids in Fig. 9a, an eight-colored scheme works as in Fig. 9b.

As will be seen in Section 5, the whole process time is dominated by the mesh generation time. The average time to generate Delaunay triangulation is $O(N \log N)$ for a N-size point set [50]. With regard to a M-decomposition scheme with the overlap ratio μ, the time to process M subdomains sequentially is $O(\mu N \log \frac{\mu N}{M})$. If well-balancedly computed on a L-united parallel machine, the time is $O(\mu \frac{N}{L} \log \frac{\mu N}{M})$. The comparison for these three schemes is plotted in Fig. 10, in which $N \in (10^3, 10^5)$, $M = 16$, $L = 4$, and $\mu = 1.1$. This comparison is plotted based on average theoretic time complexity. The mesh generation time in practice is shown in Table 5.

In this section, a new reconstruction method based on domain decomposition was proposed. Interaction between subdomains was introduced to eliminate possible cracks and conflicts. Subject to this indispensable interaction, the

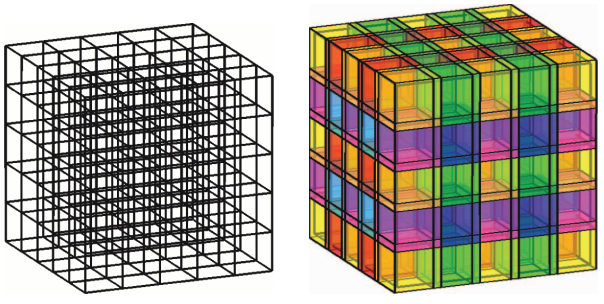

(a) regular grid decomposition (b) a coloring scheme of eight colors

Fig. 9. Eight coloring scheme.

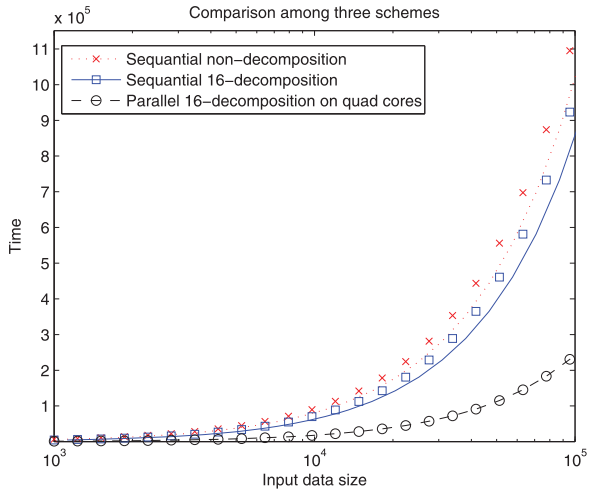

Fig. 10. Theoretic mesh time comparison among Three Schemes.

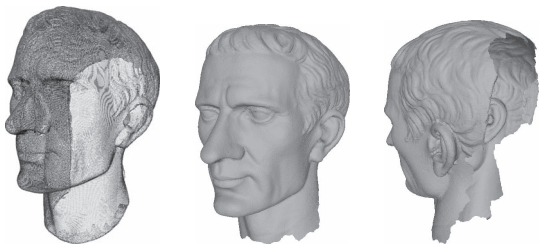

(a) Point Set (b) Result View 1 (c) Result View 2

Fig. 11. Julius Caesar.

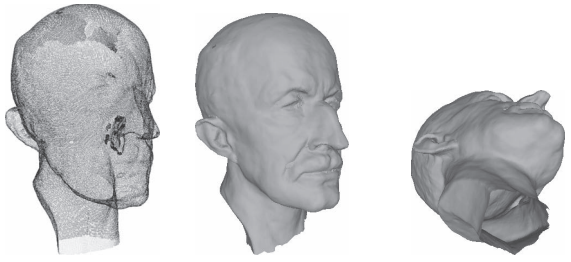

(a) Point Set (b) Result View 1 (c) Result View 2

Fig. 12. Max Planck.

feasibility of parallel implementation is discussed for some decomposition schemes. And the parallel efficiency is derived from the theoretical average time complexity of mesh generation. Some examples approached by decomposition are included in Section 5.

5 Examples

In this section, various examples are presented to demonstrate the efficiency and robustness of our method. All experiments had been conducted on a desktop PC with Intel Pentium 4 CPU of 3.2 GHz. Most models were obtained from Stanford 3D Scanning Repository, Large Geometric Models Archive of Georgia Institute of Technology and Digital Shape Workbench Project while the others were synthesized by ourselves. Computational Geometry Algorithms Library [51] is used for Delaunay triangulation; the fast algorithm in [45] is used for graph cuts; and Meshlab is used for rendering display. Based on the properties and purposes of theirs, these examples are categorized into four groups: simple open surfaces, complicated (general) surfaces, watertight surface approached by domain decomposition, and nonorientable surfaces approached by domain decomposition.

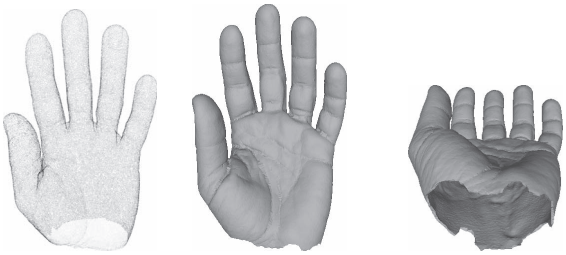

(a) Point Set (b) Result View 1 (c) Result View 2

Fig. 13. A hand model.

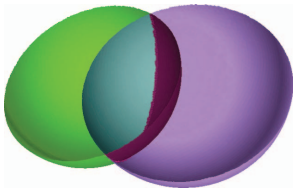

Fig. 14. A multiphase open surface example.

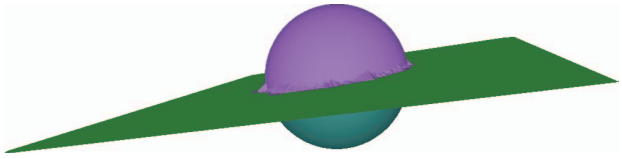

(a) A sphere intersecting a sphere

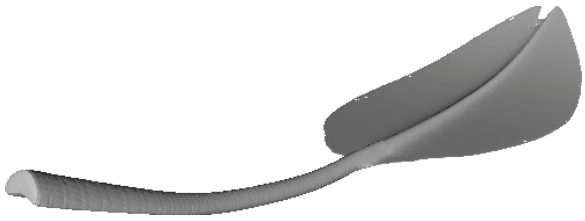

(b) A leaf model

Fig. 15. Hybrids of a watertight surface and an open one.

5.1 Simple Open Surfaces

Simple open surfaces generally refer to manifolds with boundaries. As the initial motivation of this study, several examples of the simple open surfaces are demonstrated including the data point sets and the reconstructed surfaces. Two human faces, one representative category of open surfaces, are shown in Figs. 11 and 12. The front view shows the well-preserved features and the back or bottom view shows the boundaries of reconstructed surfaces. The other example, a hand, is presented in Fig. 13.

5.2 Complicated (General) Surfaces

More general surface examples are presented in this section: multiphase open surfaces, hybrids of open and watertight surfaces, and open surfaces with noises or outliers.

An example of two intersecting semispheres, which is no longer 2-manifold, is shown in Fig. 14. Examples of hybrids of open and watertight surfaces are presented in Fig. 15. Fig. 15a shows a sphere intersecting a plane. Fig. 15b shows a real instance, a large leaf. The stalk is a watertight surface and the leaf is an open one.

(a) Photo (b) Result View 1 (c) Result View 2

Fig. 16. A real example: Khmer's Smile.

(a) Point Set (b) Result

Fig. 17. A hand model with outliers.

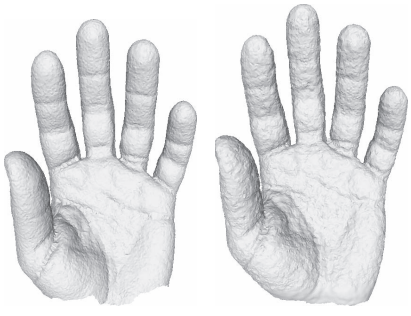

(a) Noise of $0.3\bar{h}$ (b) Noise of $0.6\bar{h}$

Fig. 18. A hand model with Gaussian noises.

Next are noisy examples. Fig. 16 shows a real example, in which the Buddha statuette is scanned incompletely with noises. Fig. 16a is the photo and Figs. 16b and 16c are reconstructed result. Fig. 17 shows an open surface example with outliers. Fig. 17a is 53,054 data points in blue and 447 outliers in red. Fig. 17b is the clean reconstructed result. Fig. 18, the last example in this section, shows examples with Gaussian noises. Fig. 18a is the result under a Gaussian noise of $0.3\bar{h}$ standard deviation and Fig. 18b under a $0.6\bar{h}$ noise.

5.3 Watertight Surfaces Approached by Domain Decomposition

Surface reconstruction based on domain decomposition is an important application of the open surface reconstruction method. In this section, some classic watertight cases are approached by the decomposition-based method. In Fig. 19, a perforated cube as well as a combination of such shapes is reconstructed in a decomposition way. In Fig. 20, two classic

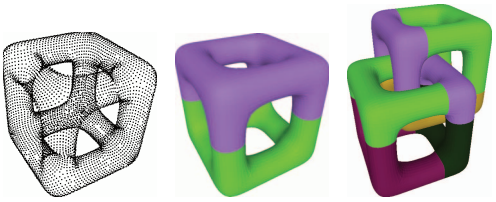

(a) (b) (c)

Fig. 19. Perforated cubes examples.

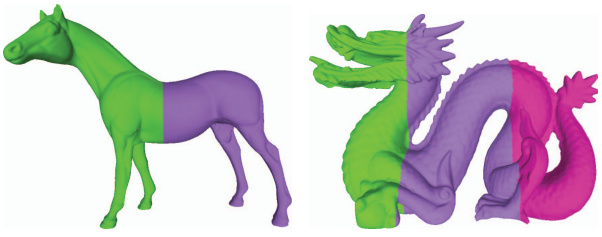

(a) Horse (b) Dragon

Fig. 20. Two classical examples.

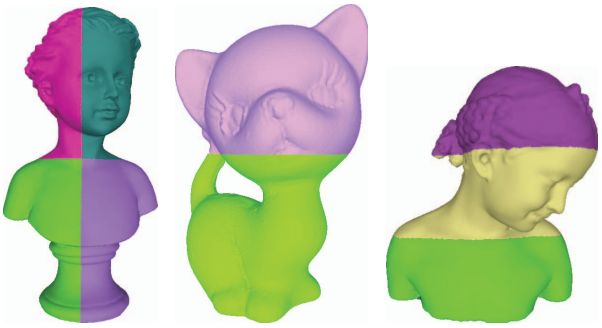

(a) Boy (b) Kitten (c) Bimba

Fig. 21. Three statuettes approached in different decomposition schemes.

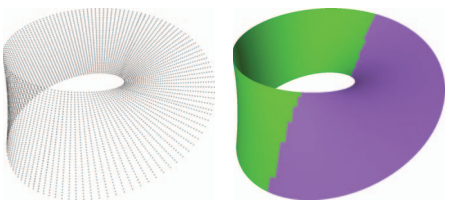

(a) Point Set (b) Result

Fig. 22. Mobius strip approached by decomposition.

examples, horse and dragon, are shown. At last of this section, three statuettes are shown in Fig. 21. From left to right, the statuettes are reconstructed in four, two, and three subdomains, respectively.

5.4 Nonorientable Surfaces

In this section, Mobius strip, one motivation of this decomposition based method, is approached perfectly with the result shown in Fig. 22. Another famous nonorientable surface, Klein bottle, is also presented in Fig. 23.

Table 4 gives the sizes of the data sets of several open surface examples and corresponding CPU time counted in seconds. The first column gives the examples' names. The second column contains the numbers of data points P. The third column is the mesh generation time, the fourth

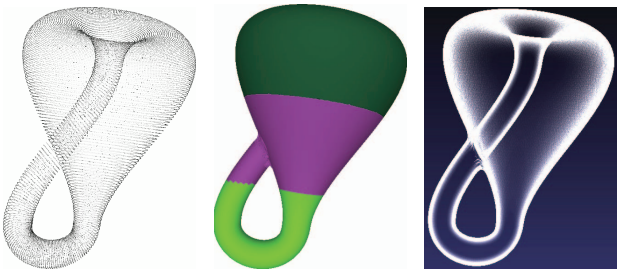

(a) Point Set (b) Result View 1 (c) Result View 2

Fig. 23. Klein bottle approached by decomposition.

TABLE 4
Statistics of Open Surface Examples

Example	Data Set	Mesh Generation Time	Graph Built Time	Graph Cut Time
Caesar	387900	248.4952	7.48386	22.3256
Planck	199169	96.7383	5.2332	9.8995
Hand	53054	41.37467	1.16082	8.49171

TABLE 5
Statistics of Domain Decomposition Examples

Example	Data Set	Mesh Generation Time	Graph Built Time	Graph Cut Time
Horse				
Non-decomposition	494195	508.4863	10.5554	5.14322
Decomposition Total	538173	465.39619	11.51025	13.97792
Subdomain 1	260881	174.86369	5.73813	10.8264
Subdomain 2	277292	290.5325	5.77212	3.15152
Dragon				
Non-decomposition	437645	383.6336	9.01963	62.0126
Decomposition Total	525939	364.8508	23.0205	27.95584
Subdomain 1	166461	118.99009	11.51025	13.97792
Subdomain 2	219725	153.18178	5.73813	10.8264
Subdomain 3	139753	92.67893	5.77212	3.15152

the graph construction time, and the fifth the graph cut time. In Table 5, included are sizes and time of the domain decomposition examples as well as those of the nondecomposition scheme. Each block contains the statistics of every subdomain as well as those in total.

6 Conclusion

In this paper, a variational reconstruction method for open surface is proposed based on graph cuts. The proposed method could robustly reconstruct not only open surfaces but also more general surfaces such as the hybrids of open and watertight ones. Surface reconstruction based on domain decomposition, as an important application, is also presented. Certain measures are taken to eliminate cracks and conflicts on the interface. Parallel efficiency is discussed as well. Parallel implementation of this domain decomposition method and investigation of its efficiency is one of our future research interests.

Acknowledgments

The authors would like to thank the referees for valuable suggestions on the improvement of the paper. This research is sponsored by Singapore MOE ARC 29/07 T207B2202, MOE RG 59/08 M52110092, and NRF 2007IDM-IDM 002-010.

References

[1] T. Dey, *Curve and Surface Reconstruction: Algorithms with Mathematical Analysis*, pp. 6-7. Cambridge Univ Press, 2007.
[2] H. Edelsbrunner and E. Mucke, "Three-Dimensional Alpha Shapes," *Proc. Workshop Vol. Visualization*, pp. 75-82, 1992.
[3] N. Amenta, M. Bern, and M. Kamvysselis, "A New Voronoi-Based Surface Reconstruction Algorithm," *Proc. 25th Ann. Conf. Computer Graphics and Interactive Techniques*, pp. 415-421, 1998.
[4] F. Bernardini, J. Mittleman, H. Rushmeier, C. Silva, and G. Taubin, "The Ball-Pivoting Algorithm for Surface Reconstruction," *IEEE Trans. Visualization and Computer Graphics*, vol. 5, no. 4, pp. 349-359, Oct.-Dec. 1999.
[5] U. Adamy, J. Giesen, and M. John, "New Techniques for Topologically Correct Surface Reconstruction," *Proc. Conf. Visualization '00*, pp. 373-380, 2000.
[6] T.K. Dey and S. Goswami, "Tight Cocone: A Water-Tight Surface Reconstructor," *Proc. Eighth ACM Symp. Solid Modeling and Applications (SM '03)*, pp. 127-134, 2003.
[7] M. Zhao, "Implicit and Nonparametric Shape Reconstruction from Unorganized Data Using a Variational Level Set Method," *Computer Vision and Image Understanding*, vol. 80, no. 3, pp. 295-314, 2000.
[8] E. Franchini, S. Morigi, and F. Sgallari, "Implicit Shape Reconstruction of Unorganized Points Using PDE-Based Deformable 3D Manifolds," *Numerical Math.: Theory, Methods and Applications*, vol. 3, pp. 405-430, 2010.
[9] H. Hoppe, T. DeRose, T. Duchamp, J. McDonald, and W. Stuetzle, "Surface Reconstruction from Unorganized Points," *Proc. 19th Ann. Conf. Computer Graphics and Interactive Techniques (SIGGRAPH '92)*, pp. 71-78, 1992.
[10] M. Alexa, J. Behr, D. Cohen-Or, S. Fleishman, D. Levin, and C. Silva, "Point Set Surfaces," *Proc. IEEE Conf. Visualization*, vol. 1, pp. 21-28, 2001.
[11] H. Zhao, S. Osher, and R. Fedkiw, "Fast Surface Reconstruction Using the Level Set Method," *Proc. IEEE Workshop Variational and Level Set Methods (VLSM '01)*, pp. 194-201, 2001.
[12] E. Franchini, S. Morigi, and F. Sgallari, "Segmentation of 3D Tubular Structures by a PDE-Based Anisotropic Diffusion Model," *Proc. Seventh Int'l Conf. Math. Methods for Curves and Surfaces*, pp. 224-241, 2010.
[13] J. Barhak and A. Fischer, "Parameterization and Reconstruction from 3D Scattered Points Based on Neural Network and pde Techniques," *IEEE Trans. Visualization and Computer Graphics*, vol. 7, no. 1, pp. 1-16, Jan.-Mar. 2001.
[14] J. Solem and A. Heyden, "Reconstructing Open Surfaces from Unorganized Data Points," *Proc. IEEE CS Conf. Computer Vision and Pattern Recognition*, vol. 2, 2004.
[15] A. Jalba and J. Roerdink, "Efficient Surface Reconstruction Using Generalized Coulomb Potentials," *IEEE Trans. Visualization and Computer Graphics*, vol. 13, no. 6, pp. 1512-1519, Nov.-Dec. 2007.
[16] R. Paulsen, J. Baerentzen, and R. Larsen, "Markov Random Field Surface Reconstruction," *IEEE Trans. Visualization and Computer Graphics*, vol. 16, no. 4, pp. 636-646, July/Aug. 2009.
[17] K. Zhou, M. Gong, X. Huang, and B. Guo, "Data-Parallel Octrees for Surface Reconstruction," *IEEE Trans. Visualization and Computer Graphics*, vol. 17, no. 5, pp. 669-681, May 2011.
[18] S. Paris, F. Sillion, and L. Quan, "A Surface Reconstruction Method Using Global Graph Cut Optimization," *Int'l J. Computer Vision*, vol. 66, no. 2, pp. 141-161, 2006.
[19] G. Zeng, S. Paris, L. Quan, and F. Sillion, "Accurate and Scalable Surface Representation and Reconstruction from Images," *IEEE Trans. Pattern Analysis and Machine Intelligence*, vol. 29, no. 1, pp. 141-158, Jan. 2007.
[20] V.S. Lempitsky and Y. Boykov, "Global Optimization for Shape Fitting," *Proc. IEEE Conf. Computer Vision and Pattern Recognition (CVPR)*, 2007.
[21] S. Paris, F. Sillion, and L. Quan, "A Surface Reconstruction Method Using Global Graph Cut Optimization," *Int'l J. Computer Vision*, vol. 66, no. 2, pp. 141-161, 2006.
[22] A. Hornung and L. Kobbelt, "Robust Reconstruction of Watertight 3D Models from Non-Uniformly Sampled Point Clouds without Normal Information," *Geometry Processing '06: Proc. Fourth Eurographics Symp. Geometry Processing*, p. 41, 2006.
[23] S. Osher and R. Fedkiw, *Level Set Methods and Dynamic Implicit Surfaces*. Springer Verlag, 2002.

[24] Y. Yu, "Surface Reconstruction from Unorganized Points Using Self-Organizing Neural Networks," *Proc. IEEE Visualization,* vol. 99, pp. 61-64, 1999.

[25] C. Kuo and H. Yau, "A Delaunay-Based Region-Growing Approach to Surface Reconstruction from Unorganized Points," *Computer-Aided Design,* vol. 37, no. 8, pp. 825-835, 2005.

[26] J. Solem and A. Heyden, "Reconstructing Open Surfaces from Image Data," *Int'l J. Computer Vision,* vol. 69, no. 3, pp. 267-275, 2006.

[27] T. Kohlberger, C. Schnörr, A. Bruhn, and J. Weickert, "Domain Decomposition for Parallel Variational Optical Flow Computation," *Proc. 25th German Conf. Pattern Recognition,* pp. 196-203, 2003.

[28] T. Kohlberger, C. Schnörr, A. Bruhn, and J. Weickert, "Domain Decomposition for Nonlinear Problems: A Control-Theoretic Approach," technical report, Computer Science Series, 2005.

[29] T. Kohlberger, C. Schnörr, A. Bruhn, and J. Weickert, "Parallel Variational Motion Estimation by Domain Decomposition and Cluster Computing," *Proc. Eighth European Conf. Computer Vision (ECCV '04),* pp. 205-216, 2004.

[30] X. Tai and J. Xu, "Global and Uniform Convergence of Subspace Correction Methods for Some Convex Optimization Problems," *Math. of Computation,* vol. 71, no. 237, pp. 105-124, 2002.

[31] Y. Duan and X. Tai, "Domain Decomposition Methods with Graph Cuts Algorithms for Total Variation Minimization," *Advances in Computational Math.,* pp. 1-25, 2011.

[32] P. Strandmark and F. Kahl, "Parallel and Distributed Graph Cuts by Dual Decomposition," *Proc. IEEE Conf. Computer Vision and Pattern Recognition (CVPR),* pp. 2085-2092, 2010.

[33] M. Wan, Y. Wang, and D. Wang, "Variational Surface Reconstruction Based on Delaunay Triangulation and Graph Cut," *Int'l J. Numerical Methods in Eng.,* vol. 85, no. 2, pp. 206-229, 2011.

[34] V. Caselles, R. Kimmel, G. Sapiro, and C. Sbert, "Minimal Surfaces Based Object Segmentation," *IEEE Trans. Pattern Analysis and Machine Intelligence,* vol. 19, no. 4, pp. 394-398, Apr. 1997.

[35] V. Caselles, R. Kimmel, and G. Sapiro, "Geodesic Active Contours," *Int'l J. Computer Vision,* vol. 22, no. 1, pp. 61-79, 1997.

[36] A. Hornung and L. Kobbelt, "Hierarchical Volumetric Multi-View Stereo Reconstruction of Manifold Surfaces Based on Dual Graph Embedding," *Proc. IEEE CS Conf. Computer Vision and Pattern Recognition,* vol. 1, 2006.

[37] E. Bae and X.-C. Tai, "Graph Cut Optimization for the Piecewise Constant Level Set Method Applied to Multiphase Image Segmentation," *Proc. Second Int'l Conf. Scale Space and Variational Methods in Computer Vision (SSVM),* X.-C. Tai, K. Morken, M. Lysaker, and K.-A. Lie eds., pp. 1-13, 2009.

[38] J. Lie, M. Lysaker, and X. Tai, "A Variant of the Level Set Method and Applications to Image Segmentation," *Math. of Computation,* vol. 75, no. 255, pp. 1155-1174, 2006.

[39] P. George and H. Borouchaki, *Delaunay Triangulation and Meshing: Application to Finite Elements.* Kogan Page, 1998.

[40] R. Gray and D. Neuhoff, "Quantization," *IEEE Trans. Information Theory,* vol. 44, no. 6, pp. 2325-2383, 2002.

[41] F. Labelle and J. Shewchuk, "Isosurface Stuffing: Fast Tetrahedral Meshes with Good Dihedral Angles," *Proc. ACM SIGGRAPH '07 Papers,* p. 57, 2007.

[42] Q. Du and D. Wang, "Tetrahedral Mesh Generation and Optimization Based on Centroidal Voronoi Tessellations," *Int'l J. Numerical Methods in Eng.,* vol. 56, pp. 1355-1373, 2002.

[43] M. Wan, D. Wang, and X. Tai, "Surface Reconstruction with Feature Preservation Based on Graph-Cuts," UCLA CAM Report 12-58.

[44] V. Kolmogorov and R. Zabin, "What Energy Functions can be Minimized via Graph Cuts?" *IEEE Trans. Pattern Analysis and Machine Intelligence,* vol. 26, no. 2, pp. 147-159, Feb. 2004.

[45] Y. Boykov and V. Kolmogorov, "An Experimental Comparison of Min-Cut/Max-Flow Algorithms for Energy Minimization in Vision," *IEEE Trans. Pattern Analysis and Machine Intelligence,* vol. 26, no. 9, pp. 1124-1137, Sept. 2004.

[46] Y. Boykov, O. Veksler, and R. Zabih, "Fast Approximate Energy Minimization via Graph Cuts," *IEEE Trans. Pattern Analysis and Machine Intelligence,* vol. 23, no. 11, pp. 1222-1239, Nov. 2001.

[47] H. Ishikawa, "Exact Optimization for Markov Random Fields with Convex Priors," *IEEE Trans. Pattern Analysis and Machine Intelligence,* vol. 25, no. 10, pp. 1333-1336, Oct. 2003.

[48] R. Adams and L. Bischof, "Seeded Region Growing," *IEEE Trans. Pattern Analysis and Machine Intelligence,* vol. 16, no. 6, pp. 641-647, June 1994.

[49] E. Hodneland, X. Tai, and H. Gerdes, "Four-Color Theorem and Level Set Methods for Watershed Segmentation," *Int'l J. Computer Vision,* vol. 82, no. 3, pp. 264-283, 2009.

[50] H. Edelsbrunner and N. Shah, "Incremental Topological Flipping Works for Regular Triangulations," *Algorithmica,* vol. 15, no. 3, pp. 223-241, 1996.

[51] "Cgal, Computational Geometry Algorithms Library," http://www.cgal.org, 1997.

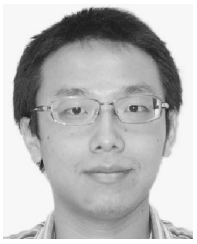

Min Wan received the BE and ME degrees in telecommunication from the Beijing University of Post and Telecom and China Academy of Telecom Technology, Beijing, China in 2004 and 2008, respectively, and is working toward the PhD degree in Nanyang Technological University. His research interests include computational geometry, computer graphics, and mesh generation.

Yu Wang received the BS and MS degrees in mathematics in 2003 and 2006 from Sichuan University. From 2006-2010, he studied computational mathematics at the School of Physical and Mathematical Sciences at Nanyang Technological University, where he received the PhD degree in 2011. He conducted research at the Department of Computer Science at Israel Institute of Technology as a postdoctoral. His research topics include numerical analysis, computational fluid dynamics, mesh generation, convex optimization, image processing, and computer graphics.

Egil Bae received the BS degree in mathematics in 2005 and the MS and PhD degrees in applied mathematics in 2007 and 2011 from the University of Bergen in Norway. He is currently a postdoctoral researcher in the mathematics Department at the University of California, Los Angeles. His research interests include optimization, variational, and PDE-based methods in image processing, computer vision, computer graphics, and machine learning.

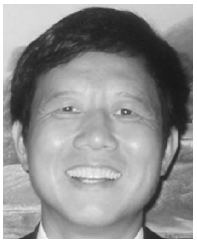

Xue-Cheng Tai received the licenciate degree and the PhD degree in applied mathematics from Jyvaskalya University, Jyvaskalya, Finland in 1989 and 1991, respectively. Since 2007, he has been with Nanyang Technological University, Singapore. After holding several research positions in Europe, he became an associate professor in 1994 at the University of Bergen, Bergen, Norway, and a professor in 1997. He has also been a part-time senior scientist at Rogaland Research. He is now a member of the Center for Mathematics for Applications in Oslo and a member of the Center of Integrated Petroleum Research in Bergen. His research interests include numerical PDE for image processing, multigrid, and domain decomposition methods, iterative methods for linear and nonlinear PDE problems, and parallel computing. He has guided numerous masters and PhD students, and published more than 80 scientific papers. He has been a reviewer and an editor for a number of international journals.

Desheng Wang received the MS degree in mathematics from Xiangtan University, Xiangtan, China, in 1997, and the PhD degree in computational mathematics from the Institute of Computational Mathematics, Chinese Academy of Sciences, Beijing, in 2001. He held a research position at Swansea University, Swansea, United Kingdom, from 2003 to 2005. Currently, he is an assistant professor with the Division of Mathematical Sciences, School of Physical and Mathematical Sciences, Nanyang Technological University, Singapore. His research interests include partial differential equation and graph-cut methods for image processing and computer vision, mesh generation, finite-element method, and computational electromagnetics.